Fabrication and characterization of mesoscopic Perovskite photodiodes

Simone Casaluci, Lucio Cinà, Fabio Matteocci, Paolo Lugli, *Member, IEEE,* Aldo Di Carlo, *Member, IEEE*

***Abstract*— Mesoscopic photodiodes were fabricated with hybrid organic/inorganic perovskite as absorber layer and Spiro-OMeTAD as Hole Transport Layer. The perovskite layer was grown using a two-step deposition technique. Our photodiode in addition to a good rectification behavior (3 orders of magnitude, range -1V to 1V) shows a small noise current (< 1pA/(Hz)$^{1/2}$), a high responsivity value (0.35 A/W) at 500 nanometers and a good spectral response in the entire visible range. The Bode analysis shows a bandwidth of 108 KHz.**

***Index Terms*— Perovskite, Photodiode, Mesoscopic, Spin coating**

I. Introduction

Recently Methylammonium lead halide $MAPbX_3$ (MA=CH_3NH_3, X=halogen) and mixed-halide perovskites compounds have attracted great attention as light absorbing materials in photovoltaic applications [1-3]. From initial power conversion efficiencies (PCEs) around 4% achieved more than five years ago [4], values as high as 20.1 % have been recently achieved [5, 6] for Perovskite solar cells (PSCs). The reason for this rapid increase in PCE is related to the excellent properties of the perovskite as light absorber (proper direct energy gap and high absorption coefficient) [7] together with an efficient carrier transport [8, 9] in the material and across the interfaces with the neighboring layers. Several techniques have been developed to grow perovskite thin films such as: i) direct deposition of the perovskite precursor solution (one-step solution deposition) on mesoscopic oxide [4, 7, 10-13] or planar oxide [14-16], ii) sequential deposition of PbI_2 and CH_3NH_3I (two step deposition) [3, 16-20]. Other deposition strategies are based on thermal sublimation in vacuum [16, 21] or vapour-assisted solution process realized for the first time by Yang group [19] and modified to reduce production cost by Casaluci [20]. When compared to standard organic solar cells based on the bulk heterojunction (BHJ) [22], PSCs share the same advantages (in terms of cost-effectiveness and solution processability) but exhibit a much higher PCE [11]. Beyond photovoltaic applications, hybrid perovskites have the required properties to become winning materials for many optoelectronic devices such as light-emitting diodes, lasers and photodetectors [23]. In particular, in this paper, we focused our attention on photodiodes, a solid-state transductor used to convert light signals into electrical signals. Compared to conventional silicon photodetectors [24], which present a wide spectral range from 400nm up to 1.1μm, hybrid perovskites have a slightly narrower band (300 nm to 800 nm for $MAPbX_3$ X=I). Nevertheless, perovskite's absorption coefficient is in the order of 10^5 cm^{-1} (at 500 nm, see figure 1d) an order of magnitude larger than Silicon [2, 25]. Thus, a perovskite thickness of 300 nm is enough to absorb most of the photons impinging on the photodiode. Several attempts have been devoted to the fabrication and characterization of perovskite-based photodiodes and photodetectors (PPD) [25-41]. In particular, the engineering of the layers surrounding the perovskite, like hole and transport materials, is essential to obtain photodetectors with superior quality. Sutherland [27] and Liu [39] investigated the electron transport material (ETM) such as TiO_2, Al_2O_3, PCBM to reduce the dark current, comparing magnetron sputtering, atomic layer deposition and spin coating techniques. For a two-step deposited inverted structure, PbS quantum dots [40], PEDOT [25] or OTPD [41] were studied as ETM, while for single step deposition, an optimization procedure was presented to improve the performance, considering BCP and PFN on PCBM as hole transport material (HTM) [38]. PPDs demonstrate a high photoconductive gain and a high responsivity [31] also for UV light [33] or with graphene implementation [30] and a fast response on flexible substrate [28] as well.

This work presents the fabrication and characterization of a $CH_3NH_3PbI_3$ PPD realized with two step deposition and Spiro-OMeTAD as HTM. For the first time, the performance of PPD with titania compact layer as ETL fabricated by spray pyrolysis will be analyzed. A thorough static and dynamic analysis will be performed to extract the important features of our device. Our PPDs show superior performance in terms of responsivity at 500 nm with respect to similar architecture PPDs [32], comparable dark current (at 0V) and detectivity with respect to non-printed PPDs [27].

We acknowledge "Polo Solare Organico" Regione Lazio and "Vigoni" Program.

S. Casaluci, L. Cinà, F. Matteocci, A. Di Carlo* are with CHOSE (Center for Hybrid and Organic Solar Energy), Department of Electronic Engineering, University of Rome "Tor Vergata" via Giacomo Peroni 400-402, 00131 Rome, Italy, (*e-mail:aldo.dicarlo@uniroma2.it).

P. Lugli is with Institute for Nanoelectronics, Technische Universitaet Muenchen, Arcisstrasse 21, 80333 Munich.

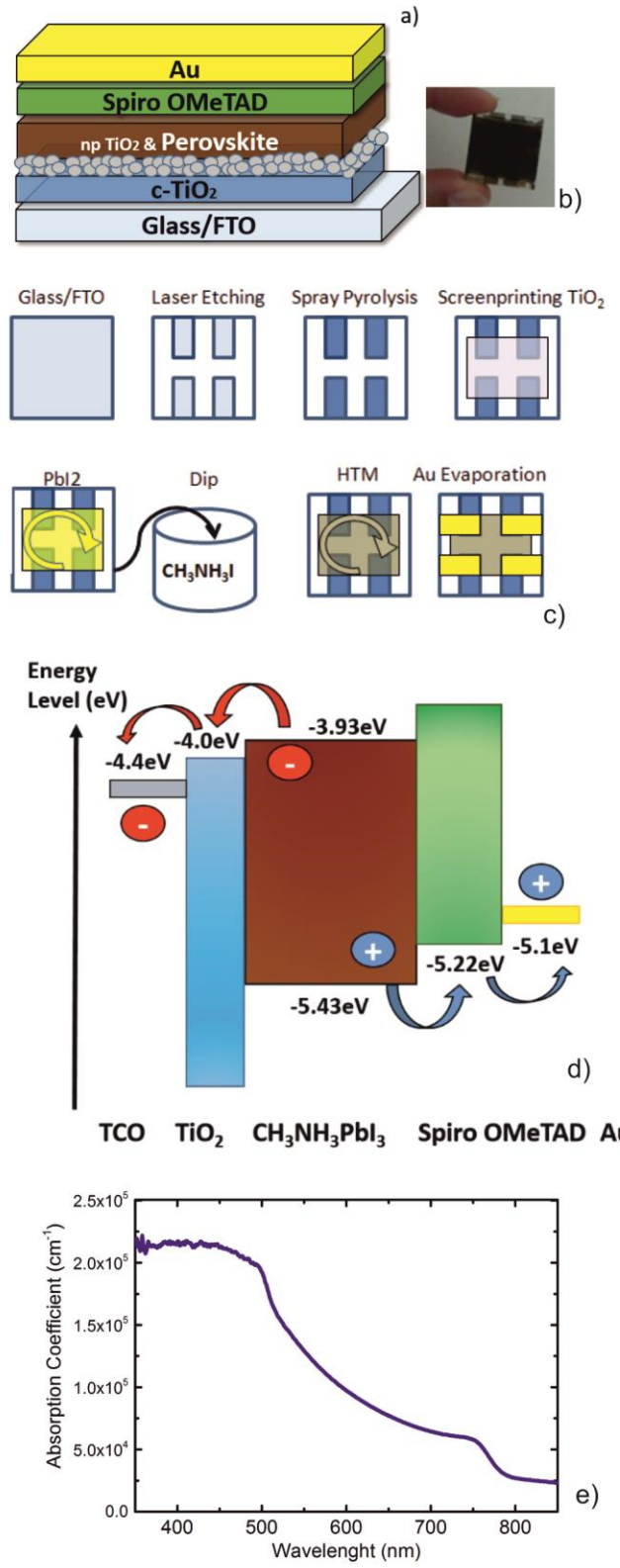

Fig. 1. a) PPD device structure and b) device photo; c) Layout of the cells and fabrication steps of the PPD. d) band alignment of the materials forming the PPD; e) absorption coefficient of the $CH_3NH_3PbI_3$ perovskite.

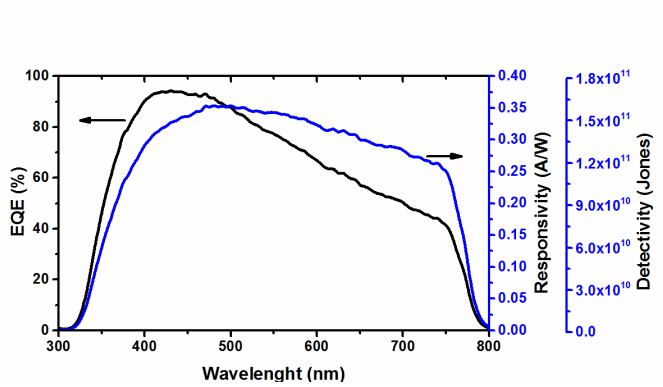

Fig. 2. EQE, responsivity at zero bias and detectivity of the fabricated PPD

II. Fabrication Steps

In order to achieve the desired electrode pattern, transparent glass substrates pre-coated with FTO (Pilkington, 8 Ohm/Square, 25 mm x 25 mm) were etched via raster scanning laser (Nd:YVO_4 pulsed at 30 kHz with average output power of P =10 W). Patterned substrates were cleaned by ultrasonic bath, using detergent, acetone and isopropanol. A compact TiO_2 (c-TiO_2) film was deposited onto the FTO surface by Spray Pyrolysis Deposition (SPD) technique [42] to obtain a compact ETL. The latter was realized using a new formulation, by adding acetylacetone (ACAC) to a conventional formulation: this enhances the c-TiO_2 adhesion over the FTO reducing the charge transfer resistance at the FTO/c-TiO_2 interface [42]. A thin film of TiO_2 nanoparticles (np-TiO_2) based paste (18NR-T Dyesol diluted with terpineol, ethilcellulose, isopropanol and ethanol) was screen-printed onto the ETL and successively sintered at 480 °C for 30 min. The final thickness of the mesoscopic np-TiO_2 (300 nm) film was measured via profilometer (Dektak Veeco 150). This layer acts as scaffold for the growth of the perovskite layer. Methylammonium iodide (Dyesol) and PbI_2 (Aldrich, 98%) were used as received. The two-step procedure involves the PbI_2 dissolved in DMF (420 mg/ml), then deposited by spin coating on the mesoporous TiO2 at 3000 rpm for 40 s, and dried at 100°C for 10 min. During the spinning of PbI_2, an airflow was applied onto the spin-coater chunk to obtain a fast drying of the sample. After, the substrate was dipped in a solution of CH_3NH_3I in 2-propanol (10 mg/ml) for 10 minutes, and dried at 70 °C for 10 minutes. The hole-transporting layer (HTL) was deposited spin coating a solution of 2,20,7,70-tetrakis-(N,N-dipmethoxyphenylamine) 9,90-spirobifluorene (Spiro-OMeTAD) at 2000 rpm for 60 s in ambient conditions and left in air overnight in a closed box containing silica desiccant. $LiN(CF_3SO_2)_2N$ and 4-tert-butylpyridine (TBP) were added in HTL solution. Samples were introduced into a high vacuum chamber (10^{-6} mbar) in order to evaporate Au electrode (thickness 100 nm) by thermal evaporation through a shadow mask. Each PPD has an active area of 0.1 cm^2. The device structure of our photodiode and its photograph are show in figure 1a and 1b. In figure 1c the chronological fabrication steps described before are reported. Figure 1d shows the band alignment diagram of the PPD structure. The light is absorbed in the perovskite active layer

This article has been accepted for publication in a future issue of this journal, but has not been fully edited. Content may change prior to final publication. Citation information: DOI 10.1109/TNANO.2016.2517239, IEEE Transactions on Nanotechnology

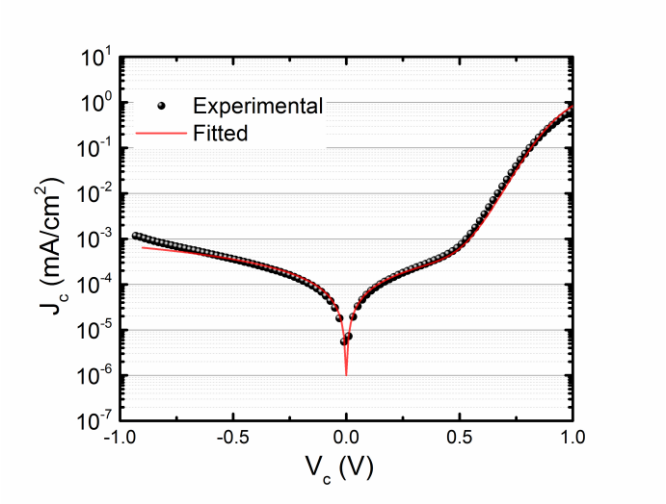

Fig. 3. Experimental and fitted JV of the PPD in dark conditions.

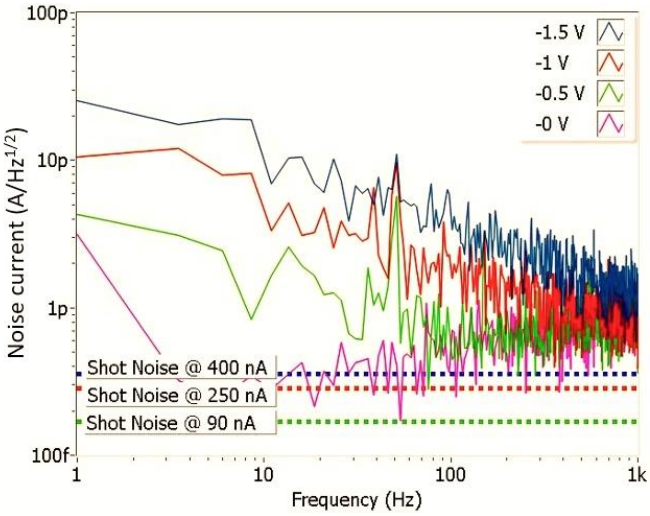

Fig. 4. Noise spectral density of the dark current at different bias. The corresponding theoretical shot noise was reported with dashed lines

and electron-hole pairs are generated. Owing to the large diffusion length, charges can easily reach the HTL and ETL where they are selected and transported to the external contacts (gold and FTO). Thus, the HTL and the ETL act as selector layers, necessary to reduce the recombination in the active layer [43] and to optimize the performance in term of charge extraction. All measurements were performed in air without encapsulation. JV measurements were performed with a scan rate of 1 mV/s (from 0V to -1V and return from 0V till 1V) and step of 10mV to reduce the hysteresis phenomena as reported by Garcia-Belmonte group [44]. Before starting the scan, the device was kept at 0V for 5 min in order to prevent capacitive effects associated to electrode polarization [45] and ions migration [46]. Detectivity and EQE seem not to be affected by hysteresis, due to the absence of bias (0V) and the slowness of the test (2nm/s for a total time of 4 minutes). Noise spectra were acquired with PXI based platform (24 bits delta sigma ADC - NI4462) connected to a low noise transimpedance amplifier (FEMTO DLPCA-200). The sample was shielded inside an aluminum enclosure. FFT elaboration was implemented with LabVIEW software. The final spectrum comes from an RMS average of 150 spectra sampled at 131 KHz for 2s (262000 samples) resulting on 5 minutes of total acquisition time.

III. Analysis

A. *Static Analysis*

To characterize the fabricated PPD we measured the external quantum efficiency (EQE) and we calculated the Responsivity (R) and the Detectivity (D) from photocurrent and dark current measurements. The EQE is the ratio between the charge collected at the contact per second and the number of photons incident per second on the active material for a given wavelength (λ). Large values of EQE in the visible and Near-Infrared (NIR) spectra (300nm-800nm) are desirable for the design of broadband photodetector able to increase the transmission capacity [47]. The responsivity R (A/W), a parameter directly connected to the EQE, gives indications on the intensity of the photocurrent that can be extracted per watt of incident optical radiation at a given λ, while the detectivity (Jones or cm $Hz^{1/2}W^{-1}$) shows the capability of the devices to detect weak signals [48]. Figure 2 shows a typical measured external quantum efficiency of our PPD in the range 300 nm - 800 nm, together with the responsivity R and detectivity D. Responsivity is calculated as

$$\frac{(EQE)\,q}{hf} = R \tag{1}$$

q is the electron charge, *f* is the frequency of optical source and *h* the Plank constant, while the detectivity is calculated as [49]

$$\frac{\sqrt{(A\,f)}\,R}{in} = D \tag{2}$$

A is the active area of device, *f* is the electrical bandwidth, and *in* is the noise current (for details see section dynamic analysis). As shown in figure 2, R and then D parameters tend to remain almost flat as the λ increases while EQE has a decreasing trend. This is due to the reduction of the photon energy incoming on the device when λ increases that compensates the EQE drop. In our PPD, R at 500nm is 0.35 A/W higher than the typical silicon photodiode responsivity [24]. On the other hand, detectivity at 530 nm and 0V was calculated to be 1.53 10^{11} Jones, a value that is still one-two orders of magnitude lower with respect to Silicon photodiode [49]. Dark current has a huge impact on detectivity parameter; a photodetector with lower dark current is able to detect smaller signals since D is proportional $(J_{dark})^{-1/2}$ [27, 38, 48]. To further investigate this issue, figure 3 shows the JV characteristics in dark conditions (for more details see fabrication step section) where Vc and Jc are the electrical parameters of the cell. A rectification ratio of about 10^3 was measured at +/- 1 V with a dark current at -1 V (reverse bias) of 1.16 10^{-3}mA/cm^2. Moreover, the good behavior of the PPD is demonstrated by low dark current (10^{-6} to 10^{-4} mA/cm^2) from

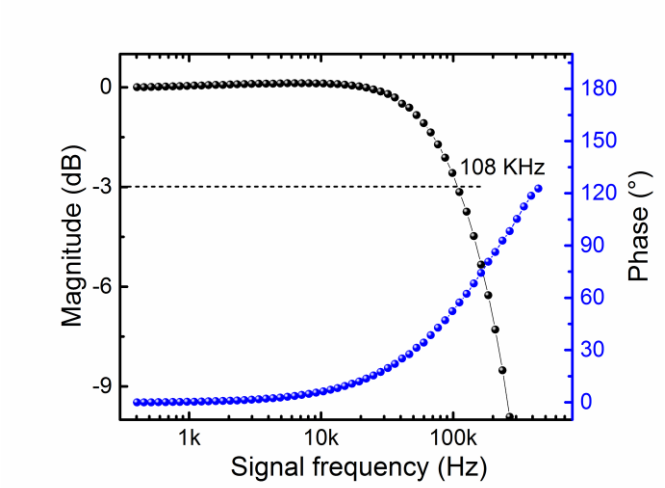

Fig. 5. Bode diagram (Magnitude and Phase) associated to optical modulation (input) and photocurrent signal (output).

TABLE I
PARAMETERS EXTRACT FROM THE JV MODEL

Parameter	Value
η (Ideally factor)	1.97
Rs (Series Resistance)	0.105 Ω/cm^2
Rsh (Shunt Resistance)	1.39 10^3 Ω/cm^2
J_0 (Saturation Current)	1.16 10^{-8} mA/cm^2

0V to -0.5V, a typical range for low noise and low voltage photodiode [27]. To extract the dark saturation current density (J_0), the dark JV curve was fitted with diode's relation (3)

$$J_0 \cdot \left[1 - e^{\left(\frac{Vc - Rs \cdot Jc}{\eta \cdot Vt}\right)}\right] + \frac{V_c - J_c \cdot R_s}{R_{sh}} = J_c \qquad (3)$$

where η is the ideality factor, R_s and R_{sh} are the series and shunt resistances, respectively, V_t the thermal voltage and J_0 is the dark saturation current density. J_0 is directly related to the recombination rate in semiconductors and to band-to-band thermal emission that limit the detectivity performance.

As reported in table I, our device shows a J_0 of 10^{-8} mA/cm^2 that is between conventional semiconductor diodes fabricated with CIGS (6 10^{-7} mA/cm^2) and those fabricated with CdTe (8 10^{-11} mA/cm^2) [50]. A better interface engineering is required in order to reduce leakage paths. Dark current can also be reduced by increasing the shunt resistance R_{sh} (10^3 Ω/cm^2 in our case) or, in other words, by reducing the recombination current that is an intrinsic characteristic of the semiconductor materials and heterojunction devices. The ideality factor η is a measure of how closely the diode follows the ideal diode equation (η =1) [51]. Trap-assisted recombination can change the ideality factor up to a value of 2. Our device shows a value of 1.97 demonstrating that the recombination paths in solution-processed perovskite based devices are assisted by trap states as demonstrated previously [52].

B. *Dynamic Analysis*

The detectivity is mainly limited by three different noise components: thermal noise, shot noise from the dark current and 1/f or Flicker noise [53]. In figure 4 we reported shot noise level for -0.5V (90nA green plot), -1.0V (250nA red plot) and -1.5V (400nA blue plot). The spectral noise density recorded at 0V (pink plot) has no corresponding shot noise level in the image. Noise spectra shown in Figure 4, denote an evident bias dependence due to an increase of dark current and, hence, on shot noise; a 1/f contribution appears for biases higher than 0.5V. A very small noise current (<1 pA/(Hz)$^{1/2}$) is achieved at 0V which is one order of magnitude smaller than silicon diodes [54]. Hence, PPD in self-powered condition (0V) can achieve a better detectivity, up to 10^{11} Jones.

To evaluate the minimum power of incident optical radiation that the PPD can discriminate from the noise, at a given λ, we calculate the noise equivalent power (NEP). The NEP at 530 nm and 0V was calculated as [38]

$$\frac{in}{R} = NEP \qquad (4)$$

For our devices, NEP was found to be 2 pW/(Hz)$^{1/2}$, only one order of magnitude higher than low noise PPD [25].

Dynamic response of the device was investigated by modulating a green led (530nm +/- 2nm) with a sinusoidal current excitation while monitoring the photocurrent in short circuit condition. The magnitude and phase plot of the frequency response of the PPD is shown in the Bode plot of Figure 5. A cut–off frequency of 108 kHz was measured. This value is higher than the cut-off frequency reported for a fully printed organic photodetector (20 KHz) [55] but lower than planar PPD optimized for bandwidth which can achieve a cut-off frequency up to 1 MHz [38]. A possible reason for the low speed is the slow response of the HTL, probably due to the lithium salt-doped Spiro-OMeTAD and the hysteresis phenomena that afflict this architecture in photovoltaic mode [56].

IV. CONCLUSION

In this work we have presented the fabrication steps and the characterization of mesoscopic Perovskite based photodiodes. Differently to other PPDs, our device has been realized by using a mesoscopic scaffold of TiO_2 and a printed ETL. A high value of external quantum efficiency is reported in the range from 300 nm to 800nm. A responsivity as high as 0.35 A/W was measured at 500nm, which outperform typical silicon photodiodes. A very small noise current (<1 pA/(Hz)$^{1/2}$) was measured at 0V, which is one order of magnitude smaller than silicon diodes. This suggests the use of PPDs in a self-powered configuration with a detectivity up to 10^{11} Jones. Frequency

analysis demonstrated a bandwidth of 108 kHz. We believe that the bandwidth may be further improved by reducing the active area of the device in order to decrease the device capacitance and resistance as already demonstrated by Dou [38]. Moreover, due to a well known poor ambient condition stability of perovskite materials, to evaluate the performance of PPD on longtime scale an encapsulation of the device is necessary.

The application of hybrid perovskites in mesoscopic photodiodes shows promising performances that can be further optimized by reducing the dark current. The optimization strategy we are following aims at the use of different materials for the compact layer, novel technique to grow the perovskite layer, the deposition of alternative HTL and the use of alternative counter electrodes. Our results and the foreseen improvements pave the way to implement the Perovskite-based photodiodes in low cost and high performance applications.

REFERENCES

[1] H. J. Snaith, "Perovskites: the emergence of a new era for low-cost, high-efficiency solar cells," *The Journal of Physical Chemistry Letters*, vol. 4, pp. 3623-3630, 2013.

[2] M. A. Green, A. Ho-Baillie, and H. J. Snaith, "The emergence of perovskite solar cells," *Nat Photon*, vol. 8, pp. 506-514, 07//print 2014.

[3] J. Burschka, N. Pellet, S.-J. Moon, R. Humphry-Baker, P. Gao, M. K. Nazeeruddin, *et al.*, "Sequential deposition as a route to high-performance perovskite-sensitized solar cells," *Nature*, vol. 499, pp. 316-319, 2013.

[4] A. Kojima, K. Teshima, Y. Shirai, and T. Miyasaka, "Organometal halide perovskites as visible-light sensitizers for photovoltaic cells," *Journal of the American Chemical Society*, vol. 131, pp. 6050-6051, 2009.

[5] (Accessed: September, 2015). Available: http://www.nrel.gov/ncpv/images/efficiency_chart.jpg

[6] W. S. Yang, J. H. Noh, N. J. Jeon, Y. C. Kim, S. Ryu, J. Seo, *et al.*, "High-performance photovoltaic perovskite layers fabricated through intramolecular exchange," *Science*, vol. 348, pp. 1234-1237, June 12, 2015 2015.

[7] H.-S. Kim, C.-R. Lee, J.-H. Im, K.-B. Lee, T. Moehl, A. Marchioro, *et al.*, "Lead iodide perovskite sensitized all-solid-state submicron thin film mesoscopic solar cell with efficiency exceeding 9%," *Scientific reports*, vol. 2, 2012.

[8] G. Xing, N. Mathews, S. Sun, S. S. Lim, Y. M. Lam, M. Grätzel, *et al.*, "Long-range balanced electron-and hole-transport lengths in organic-inorganic CH3NH3PbI3," *Science*, vol. 342, pp. 344-347, 2013.

[9] S. D. Stranks, G. E. Eperon, G. Grancini, C. Menelaou, M. J. Alcocer, T. Leijtens, *et al.*, "Electron-hole diffusion lengths exceeding 1 micrometer in an organometal trihalide perovskite absorber," *Science*, vol. 342, pp. 341-344, 2013.

[10] J. T.-W. Wang, J. M. Ball, E. M. Barea, A. Abate, J. A. Alexander-Webber, J. Huang, *et al.*, "Low-temperature processed electron collection layers of graphene/TiO2 nanocomposites in thin film perovskite solar cells," *Nano letters*, vol. 14, pp. 724-730, 2013.

[11] F. Di Giacomo, S. Razza, F. Matteocci, A. D'Epifanio, S. Licoccia, T. M. Brown, *et al.*, "High efficiency CH3NH3PbI(3−x)Clx perovskite solar cells with poly(3-hexylthiophene) hole transport layer," *Journal of Power Sources*, vol. 251, pp. 152-156, 4/1/ 2014.

[12] N. J. Jeon, J. H. Noh, Y. C. Kim, W. S. Yang, S. Ryu, and S. I. Seok, "Solvent engineering for high-performance inorganic–organic hybrid perovskite solar cells," *Nature materials*, 2014.

[13] M. M. Lee, J. Teuscher, T. Miyasaka, T. N. Murakami, and H. J. Snaith, "Efficient hybrid solar cells based on meso-superstructured organometal halide perovskites," *Science*, vol. 338, pp. 643-647, 2012.

[14] G. E. Eperon, V. M. Burlakov, P. Docampo, A. Goriely, and H. J. Snaith, "Morphological Control for High Performance, Solution-Processed Planar Heterojunction Perovskite Solar Cells," *Advanced Functional Materials*, vol. 24, pp. 151-157, 2014.

[15] B. Conings, L. Baeten, C. De Dobbelaere, J. D'Haen, J. Manca, and H.-G. Boyen, "Perovskite-Based Hybrid Solar Cells Exceeding 10% Efficiency with High Reproducibility Using a Thin Film Sandwich Approach," *Advanced Materials*, vol. 26, pp. 2041-2046, 2014.

[16] D. Liu and T. L. Kelly, "Perovskite solar cells with a planar heterojunction structure prepared using room-temperature solution processing techniques," *Nature photonics*, vol. 8, pp. 133-138, 2014.

[17] Y. Wu, A. Islam, X. Yang, C. Qin, J. Liu, K. Zhang, *et al.*, "Retarding the crystallization of PbI 2 for highly reproducible planar-structured perovskite solar cells via sequential deposition," *Energy & Environmental Science*, vol. 7, pp. 2934-2938, 2014.

[18] D. Bi, S.-J. Moon, L. Häggman, G. Boschloo, L. Yang, E. M. Johansson, *et al.*, "Using a two-step deposition technique to prepare perovskite (CH 3 NH 3 PbI 3) for thin film solar cells based on ZrO 2 and TiO 2 mesostructures," *Rsc Advances*, vol. 3, pp. 18762-18766, 2013.

[19] Q. Chen, H. Zhou, Z. Hong, S. Luo, H.-S. Duan, H.-H. Wang, *et al.*, "Planar heterojunction perovskite solar cells via vapor-assisted solution process," *Journal of the American Chemical Society*, vol. 136, pp. 622-625, 2013.

[20] S. Casaluci, L. Cinà, A. Pockett, P. S. Kubiak, R. G. Niemann, A. Reale, *et al.*, "A simple approach for the fabrication of perovskite solar cells in air," *Journal of Power Sources*, vol. 297, pp. 504-510, 2015.

[21] H. Hu, D. Wang, Y. Zhou, J. Zhang, S. Lv, S. Pang, *et al.*, "Vapour-based processing of hole-conductor-free CH 3 NH 3 PbI 3 perovskite/C 60 fullerene planar solar cells," *RSC Advances*, vol. 4, pp. 28964-28967, 2014.

[22] N. Sariciftci, L. Smilowitz, A. J. Heeger, and F. Wudl, "Photoinduced electron transfer from a conducting polymer to buckminsterfullerene," *Science*, vol. 258, pp. 1474-1476, 1992.

[23] Q. Chen, N. De Marco, Y. M. Yang, T.-B. Song, C.-C. Chen, H. Zhao, *et al.*, "Under the spotlight: The organic–inorganic hybrid halide perovskite for optoelectronic applications," *Nano Today*, vol. 10, pp. 355-396, 2015.

[24] S. Radovanovic, A.-J. Annema, and B. Nauta, *High-speed photodiodes in standard CMOS technology* vol. 869: Springer Science & Business Media, 2006.

[25] Q. Lin, A. Armin, D. M. Lyons, P. L. Burn, and P. Meredith, "Photodiodes: Low Noise, IR-Blind Organohalide Perovskite Photodiodes for Visible Light Detection and Imaging (Adv. Mater. 12/2015)," *Advanced Materials*, vol. 27, pp. 1969-1969, 2015.

[26] Q. Lin, A. Armin, P. L. Burn, and P. Meredith, "Filterless narrowband visible photodetectors," *Nat Photon*, vol. 9, pp. 687-694, 10//print 2015.

[27] B. R. Sutherland, A. K. Johnston, A. H. Ip, J. Xu, V. Adinolfi, P. Kanjanaboos, *et al.*, "Sensitive, fast, and stable perovskite photodetectors exploiting interface engineering," *ACS Photonics*, vol. 2, pp. 1117-1123, 2015.

[28] X. Hu, X. Zhang, L. Liang, J. Bao, S. Li, W. Yang, *et al.*, "High-Performance Flexible Broadband Photodetector Based on Organolead Halide Perovskite," *Advanced Functional Materials*, vol. 24, pp. 7373-7380, 2014.

[29] H.-R. Xia, J. Li, W.-T. Sun, and L.-M. Peng, "Organohalide lead perovskite based photodetectors with much enhanced performance," *Chemical Communications*, vol. 50, pp. 13695-13697, 2014.

[30] Y. Lee, J. Kwon, E. Hwang, C. H. Ra, W. J. Yoo, J. H. Ahn, *et al.*, "High-Performance Perovskite–Graphene Hybrid Photodetector," *Advanced Materials*, vol. 27, pp. 41-46, 2015.

[31] R. Dong, Y. Fang, J. Chae, J. Dai, Z. Xiao, Q. Dong, *et al.*, "High-Gain and Low-Driving-Voltage Photodetectors Based on Organolead Triiodide Perovskites," *Advanced Materials*, vol. 27, pp. 1912-1918, 2015.

[32] D. Li, G. Dong, W. Li, and L. Wang, "High performance organic-inorganic perovskite-optocoupler based on low-voltage and fast response perovskite compound photodetector," *Scientific reports*, vol. 5, 2015.

[33] Y. Guo, C. Liu, H. Tanaka, and E. Nakamura, "Air-Stable and Solution-Processable Perovskite Photodetectors for Solar-Blind UV and Visible Light," *The Journal of Physical Chemistry Letters*, vol. 6, pp. 535-539, 2015.

[34] R. Gottesman, E. Haltzi, L. Gouda, S. Tirosh, Y. Bouhadana, A. Zaban, *et al.*, "Extremely slow photoconductivity response of CH3NH3PbI3 perovskites suggesting structural changes under

working conditions," *The Journal of Physical Chemistry Letters*, vol. 5, pp. 2662-2669, 2014.

[35] M. He, Y. Chen, H. Liu, J. Wang, X. Fang, and Z. Liang, "Chemical decoration of CH 3 NH 3 PbI 3 perovskites with graphene oxides for photodetector applications," *Chemical Communications*, vol. 51, pp. 9659-9661, 2015.

[36] H.-W. Chen, N. Sakai, A. K. Jena, Y. Sanehira, M. Ikegami, K.-C. Ho, *et al.*, "A Switchable High Sensitivity Photodetecting and Photovoltaic Device with Perovskite Absorber," *The Journal of Physical Chemistry Letters*, 2015.

[37] Y. Zhang, J. Du, X. Wu, G. Zhang, Y. Chu, D. Liu, *et al.*, "Ultrasensitive Photodetectors Based on Island-Structured CH3NH3PbI3 Thin Films," *ACS applied materials & interfaces*, 2015.

[38] L. Dou, Y. M. Yang, J. You, Z. Hong, W.-H. Chang, G. Li, *et al.*, "Solution-processed hybrid perovskite photodetectors with high detectivity," *Nature communications*, vol. 5, 2014.

[39] C. Liu, K. Wang, C. Yi, X. Shi, P. Du, A. W. Smith, *et al.*, "Ultrasensitive solution-processed perovskite hybrid photodetectors," *Journal of Materials Chemistry C*, 2015.

[40] C. Liu, K. Wang, P. Du, E. Wang, X. Gong, and A. J. Heeger, "Ultrasensitive solution-processed broad-band photodetectors using CH 3 NH 3 PbI 3 perovskite hybrids and PbS quantum dots as light harvesters," *Nanoscale*, vol. 7, pp. 16460-16469, 2015.

[41] Y. Fang and J. Huang, "Resolving Weak Light of Sub-picowatt per Square Centimeter by Hybrid Perovskite Photodetectors Enabled by Noise Reduction," *Advanced Materials*, vol. 27, pp. 2804-2810, 2015.

[42] F. Matteocci, G. Mincuzzi, F. Giordano, A. Capasso, E. Artuso, C. Barolo, *et al.*, "Blocking layer optimisation of poly (3-hexylthiopene) based solid state dye sensitized solar cells," *Organic Electronics*, vol. 14, pp. 1882-1890, 2013.

[43] E. J. Juarez-Perez, M. Wuβler, F. Fabregat-Santiago, K. Lakus-Wollny, E. Mankel, T. Mayer, *et al.*, "Role of the Selective Contacts in the Performance of Lead Halide Perovskite Solar Cells," *The Journal of Physical Chemistry Letters*, vol. 5, pp. 680-685, 2014/02/20 2014.

[44] O. Almora, I. Zarazua, E. Mas-Marza, I. Mora-Sero, J. Bisquert, and G. Garcia-Belmonte, "Capacitive Dark Currents, Hysteresis, and Electrode Polarization in Lead Halide Perovskite Solar Cells," *The Journal of Physical Chemistry Letters*, vol. 6, pp. 1645-1652, 2015/05/07 2015.

[45] H.-S. Kim, I.-H. Jang, N. Ahn, M. Choi, A. Guerrero, J. Bisquert, *et al.*, "Control of I–V Hysteresis in CH3NH3PbI3 Perovskite Solar Cell," *The Journal of Physical Chemistry Letters*, vol. 6, pp. 4633-4639, 2015/11/19 2015.

[46] B. Chen, M. Yang, X. Zheng, C. Wu, W. Li, Y. Yan, *et al.*, "Impact of Capacitive Effect and Ion Migration on the Hysteretic Behavior of Perovskite Solar Cells," *The Journal of Physical Chemistry Letters*, pp. 4693-4700, 2015/11/09 2015.

[47] J. Bregman, R. Nagi, R. Olah, P. Oduor, and A. K. Dutta, "High performance broadband photodetector and its array for optical communication," 2015, pp. 93880Q-93880Q-6.

[48] G. Pace, A. Grimoldi, M. Sampietro, D. Natali, and M. Caironi, "Printed photodetectors," *Semiconductor Science and Technology*, vol. 30, p. 104006, 2015.

[49] X. Gong, M. Tong, Y. Xia, W. Cai, J. S. Moon, Y. Cao, *et al.*, "High-Detectivity Polymer Photodetectors with Spectral Response from 300 nm to 1450 nm," *Science*, vol. 325, pp. 1665-1667, September 25, 2009 2009.

[50] S. S. Hegedus and W. N. Shafarman, "Thin-film solar cells: device measurements and analysis," *Progress in Photovoltaics: Research and Applications*, vol. 12, pp. 155-176, 2004.

[51] C.-T. Sah, R. Noyce, and W. Shockley, "Carrier generation and recombination in pn junctions and pn junction characteristics," *Proceedings of the IRE*, vol. 45, pp. 1228-1243, 1957.

[52] G. J. A. Wetzelaer, M. Scheepers, A. M. Sempere, C. Momblona, J. Ávila, and H. J. Bolink, "Trap-Assisted Non-Radiative Recombination in Organic–Inorganic Perovskite Solar Cells," *Advanced Materials*, vol. 27, pp. 1837-1841, 2015.

[53] C. Beenakker and C. Schonenberger, "Quantum shot noise," *Physics Today* 2003.

[54] S. Malik, A. K. Ray, and S. Bruce, "1/ f noise in Langmuir–Blodgett films on silicon," *Semiconductor Science and Technology*, vol. 20, p. 453, 2005.

[55] G. Azzellino, A. Grimoldi, M. Binda, M. Caironi, D. Natali, and M. Sampietro, "Fully Inkjet-Printed Organic Photodetectors with High Quantum Yield," *Advanced Materials*, vol. 25, pp. 6829-6833, 2013.

[56] H. J. Snaith, A. Abate, J. M. Ball, G. E. Eperon, T. Leijtens, N. K. Noel, *et al.*, "Anomalous hysteresis in perovskite solar cells," *The Journal of Physical Chemistry Letters*, vol. 5, pp. 1511-1515, 2014.

Simone Casaluci was born in Rome, Italy, in 1985. He received the M.S. degree in electronic engineering from the University of Rome "Tor Vergata", Rome, in 2011 where he is currently pursuing the Ph.D. degree in Telecommunication and microelectronics engineering. His current research at Centre for Hybrid and Organic Solar Energy (CHOSE) lab interests fabrication and characterization of Perovskite solar cells and the implementation of graphene in the structure.

Lucio Cinà received the M.Sc. degree summa cum laude in Electronic Engineering at University of Rome "Tor Vergata" (Italy) in 2009 and his Ph.D. degree from the Center for Hybrid and Organic Solar Energy (CHOSE) of Lazio region in 2013. He is currently post-doc researcher of Prof. Aldo Di Carlo group (CHOSE). His research activity concerns the development of advanced electro-optical characterization systems for hybrid photovoltaic devices, in particular Perovskite based Solar Cells (PSC) and the electrochemical impedance analysis of Lithium Polymer batteries (LiPO).

Fabio Matteocci was born in Rome, (Italy) in 1983. He received the Degree in Electronic Engineering from the University of Rome "Tor Vergata" (Italy) in 2009 and his Ph.D. degree in electrical engineering from the Center for Hybrid and Organic Solar Energy (CHOSE) in 2014. He is a post-doc researcher at CHOSE lab. He is mainly working on the development of scalable realization processes for thin-film photovoltaic technologies such as solid-state DSCs and perovskite solar cell.

Paolo Lugli (M'01–SM'07–F'11) received the Degree in physics from the University of Modena, Modena, Italy, in 1979, and the M.S. and Ph.D. degrees in electrical engineering from Colorado State University, Fort Collins, CO, USA, in 1982 and 1985, respectively. He joined the University of Modena, in 1985. In 2003, he joined the Technical University of Munich, Munich, Germany, where he was appointed as the Head of the Institute for Nanoelectronics.

Aldo Di Carlo received his degree in Physics (with honors) from the University of Rome "La Sapienza" (Italy) in 1991 and his Ph.D. degree from the Technische Universität München (Germany) in 1995. He is currently a Full Professor of Optoelectronics and Nanoelectronics at the University of Rome "Tor Vergata" (Italy), and since 2006, he has also been co-director of the Centre for Hybrid and Organic Solar Energy (CHOSE). His research activity mainly concerns the study of electronic transport and optoelectronic properties of nanostructured and organic semiconductor devices and their fabrication.